Chem

CellPress

Article

Exploring mechanism of enzyme catalysis by on-chip transient kinetics coupled with global data analysis and molecular modeling

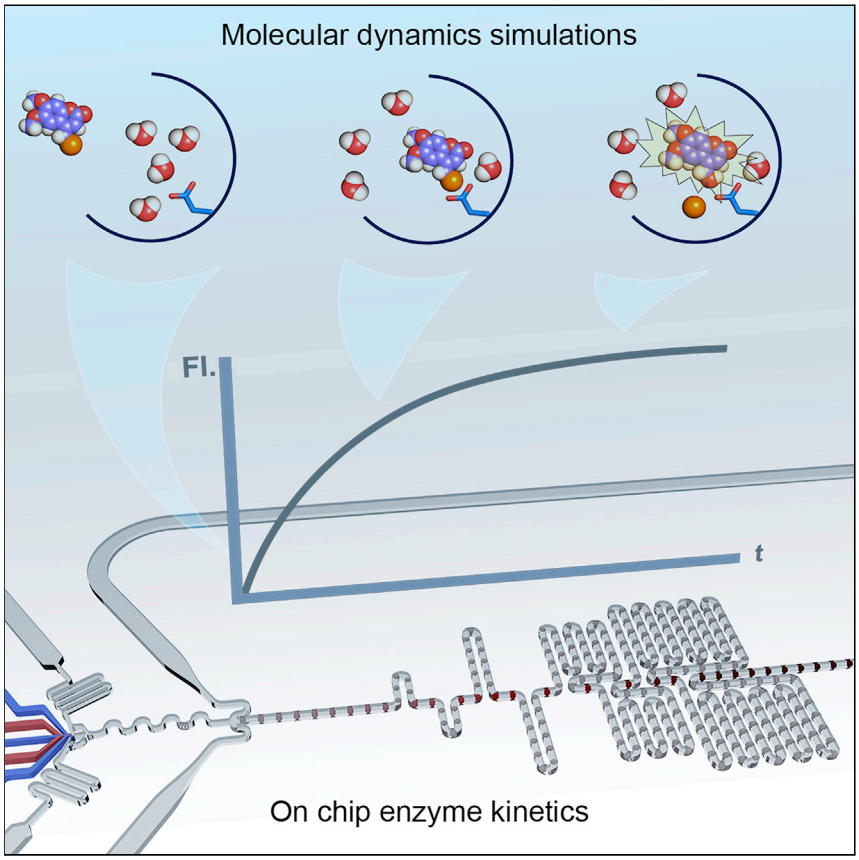

A droplet-based microfluidic platform for fast kinetic measurements and high-throughput profiling of enzymatic reactions is presented. The approach leverages the acceleration of flowing droplets to decrease mixing times, with subsequent droplet deceleration allowing for efficient droplet analysis. Single droplet resolution detection is based on stroboscopic epifluorescence imaging, with the resulting datasets, processed by global numerical methods and complemented by molecular dynamics simulations, providing insight into the reaction mechanism, and suggesting directions for the efficient design of new biocatalysts.

David Hess, Veronika Dockalova, Piia Kokkonen, ..., Andrew deMello, Zbynek Prokop, Stavros Stavrakis

andrew.demello@chem.ethz.ch (A.d.)
zbynek@chemi.muni.cz (Z.P.)
stavros.stavrakis@chem.ethz.ch (S.S.)

HIGHLIGHTS

A microfluidic platform for kinetic and thermodynamic studies of enzyme catalysis

Ultrahigh-throughput extraction of transient kinetics of enzymatic reactions

Insight into the molecular basis and thermodynamics of enzyme specificity is achieved

A detailed mechanistic and thermodynamic study of haloalkane dehalogenases is achieved

Hess et al., Chem 7, 1–14
April 8, 2021
https://doi.org/10.1016/j.chempr.2021.02.011

Please cite this article in press as: Hess et al., Exploring mechanism of enzyme catalysis by on-chip transient kinetics coupled with global data analysis and molecular modeling, Chem (2021), https://doi.org/10.1016/j.chempr.2021.02.011

Chem

CellPress

Article

Exploring mechanism of enzyme catalysis by on-chip transient kinetics coupled with global data analysis and molecular modeling

David Hess,[1,5] Veronika Dockalova,[2,5] Piia Kokkonen,[2] David Bednar,[2] Jiri Damborsky,[2,3] Andrew deMello,[1,4,*] Zbynek Prokop,[2,3,*] and Stavros Stavrakis[1,*]

SUMMARY

The ability to engineer enzymes for industrial and biomedical applications is primarily limited by a paucity of mechanistic understanding. To gain insight into the mechanisms of enzyme catalysis, one must screen enormous numbers of discrete reaction conditions, which is a laborious task using conventional technologies. To address such limitations, we develop a droplet-based microfluidic platform for high-throughput acquisition of transient kinetic data over a range of substrate concentrations and temperatures. When compared with conventional methods, our platform reduces assay volumes by six orders of magnitude and increases throughput to 9,000 reactions/min. To demonstrate their utility, we measure the transient kinetics of three model enzymes, namely, β-galactosidase, horseradish peroxidase, and microperoxidase. Additionally, we conduct a complex kinetic and thermodynamic study of engineered variants of haloalkane dehalogenases. Datasets are globally analyzed and complemented by molecular dynamics simulations, providing new insights into the molecular basis of substrate specificity and the role of hydration-related entropy.

INTRODUCTION

Enzymes exhibiting both high specificity and selectivity are highly desirable in a broad range of industrial and biomedical applications.[1,2] Despite their structural and chemical diversity, relatively few naturally occurring enzymes have been applied directly to industrial processes of relevance.[3,4] Indeed, extensive enzyme redesigning via protein engineering is almost always needed to fit process specifications.[5–7] Moreover, the accuracy of any enzyme-engineering process is primarily limited by an incomplete understanding of the mechanism of the targeted functionality.[8] In this respect, recent developments in numerical methods have begun to provide a more general framework for global analysis of complex steady-state and pre-steady-state experimental datasets (collected over a range of substrate concentrations and temperatures), with a view to providing deeper insights into the mechanism of biomolecular processes.[9,10] The primary obstacle in accessing such complex experimental datasets lies in the technical limitations of conventional (rapid-mixing) instrumentation used in pre-steady-state kinetic analysis, which include excessive sample/reagent consumption, low analytical throughput, high investment costs, and long equilibration times.[11]

Microfluidic systems are able to provide direct solutions to the aforementioned limitations, and it is thus unsurprising that a number of microfluidic platforms have

The bigger picture

Comprehensive kinetic and thermodynamic studies of enzyme specificity and catalytic efficiency require acquisition of complex kinetic data collected over a range of substrate concentrations and temperatures. The main limitations in obtaining such data sets are currently set by the timescale and material requirements associated with traditional "rapid-mixing" methods. To address these limitations, we present a high-throughput droplet-based microfluidic methodology for fast kinetic measurements and thermodynamic profiling of enzymatic reactions. The complex datasets processed by global numerical methods and complemented by molecular dynamics simulations provide detailed insight into the reaction mechanism, a key prerequisite for the efficient rational protein engineering of novel biocatalysts. To showcase the broad utility of our platform, we conducted a kinetic and thermodynamic study of engineered variants of haloalkane dehalogenases.

Please cite this article in press as: Hess et al., Exploring mechanism of enzyme catalysis by on-chip transient kinetics coupled with global data analysis and molecular modeling, Chem (2021), https://doi.org/10.1016/j.chempr.2021.02.011

already been used successfully to study millisecond kinetics by leveraging their unique features.[12,13] Key advantages of such systems include significantly reduced sample/reagent volumes, ultrahigh analytical throughput, the facile integration of different functionalities within monolithic structures, and an exquisite control of both heat and mass transport.[14] With regard to kinetic measurements, efficient heat and mass transfer ensure rapid temperature equilibration or reactant mixing, without a need for long incubation times. In turn, this enables the unbiased analysis of unstable reactants and allows thermodynamic studies of fragile enzymes by probing their properties close to or even above the denaturation temperature. Moreover, the ease of component integration, system automation, and multiplexing ensures that microfluidic tools can be used to good effect in a wide range of "high-throughput" scenarios.[15–17] Droplet-based microfluidic systems are especially well-suited for use in kinetic experiments, since the formation of segmented flows eliminates residence time distributions and prevents deleterious molecule-surface interactions.[12,13,18–21] In addition, droplet-based systems are advantageous due to their ability to rapidly generate enormous numbers of discrete droplets with user-defined payloads, to passively effect reactant mixing via chaotic advection,[13] and to directly probe individual droplets at rates well in excess of 10,000 droplets/s. Finally, the space-to-time relationship established within a segmented-flow scheme enables moving droplets to be repeatedly imaged at different locations (and thus time points) along the flow path, ensuring that integration times associated with signal acquisition are decoupled from the time resolution of the measurement itself. This in turn makes it possible to average the signal from a large number of droplets (i.e., experiments) passing a detection point to provide for enhanced sensitivities and detection limits.[22] Despite these compelling advantages and prior reports of droplet-based microfluidic systems for on-chip kinetic measurements,[23–25] there is a surprising dearth of appropriate platforms for the high-throughput extraction of (enzyme) kinetic and thermodynamic information. To this end, we present a droplet-based microfluidic platform able to perform ultrafast kinetic measurements and thermodynamic profile scans of a wide variety of enzymatic reactions. Our approach is intimately based on the acceleration of generated droplets to enhance reactant mixing (and minimize dead times) and a subsequent deceleration of mixed droplets to allow for sensitive detection of droplet contents. We initially demonstrate the broad applicability of the approach in measuring the transient kinetics of three model enzymes, namely, β-galactosidase, horseradish peroxidase, and microperoxidase. Subsequently, we use the platform to explore the mechanism underlying the catalytic efficiency of the haloalkane dehalogenase, LinB, from *Shingobium japonicum* UT26 (UniProt: D4Z2G1) and two variants with engineered access tunnels. The mechanistic study combines global kinetic data analysis using numerical methods and molecular dynamics simulations and provides critical new information regarding the role of hydration and entropy in substrate specificity, which is inaccessible to conventional techniques.

RESULTS

Design and operation of the microfluidic system

When using segmented flows, reagent mixing can be passively accelerated through chaotic advection induced by geometric turns along the flow path.[26] Using such an approach, we developed a microfluidic platform that rapidly accelerates droplets shortly after their formation at a flow-focusing geometry and before they enter a serpentine channel path to induce rapid mixing by chaotic advection (Figures 1 and S1; Supplemental experimental procedure 3.10). Once payload mixing is complete (within 1 ms), the droplet velocity is rapidly decreased by draining a portion of

[1]Institute for Chemical and Bioengineering, ETH Zürich, Vladimir Prelog Weg 1, 8093 Zürich, Switzerland

[2]Loschmidt Laboratories, Department of Experimental Biology and RECETOX, Faculty of Science, Masaryk University, Kamenice 5/A13, 625 00 Brno, Czech Republic

[3]International Clinical Research Center, St. Anne's University Hospital, Pekarska 53, 656 91 Brno, Czech Republic

[4]Lead contact

[5]These authors contributed equally

*Correspondence:
andrew.demello@chem.ethz.ch (A.d.),
zbynek@chemi.muni.cz (Z.P.),
stavros.stavrakis@chem.ethz.ch (S.S.)

https://doi.org/10.1016/j.chempr.2021.02.011

Please cite this article in press as: Hess et al., Exploring mechanism of enzyme catalysis by on-chip transient kinetics coupled with global data analysis and molecular modeling, Chem (2021), https://doi.org/10.1016/j.chempr.2021.02.011

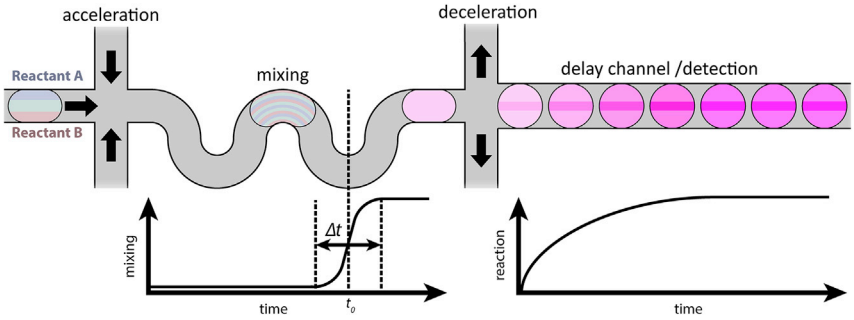

Figure 1. Schematic of the microfluidic platform and workflow for the high-throughput acquisition of transient kinetic data

Preformed droplets containing the reaction solutions are accelerated by the injection of oil flows from side channels. Droplets are subsequently driven at high velocity through a winding channel section, which acts to accelerate content mixing via chaotic advection. Subsequently, droplet velocities are reduced by removing part of the oil via sideway channels. Detection is based on stroboscopic epifluorescence imaging, whereby the excitation light is focused into a concentrated laser line illuminating the center of the droplets.

the continuous oil phase away from the primary flow, resulting in an immediate decrease in the distance between droplets. Optical analysis of droplet contents then occurs within a straight delay channel via stroboscopic light-sheet epifluorescence imaging (Figure S2).

The basic microfluidic device comprises four inlets, one for the continuous phase and three for the delivery of reaction components (Figure 2A). Typically, one input contains the enzyme, one consists of pure buffer, and one contains the reaction substrate. The use of a pure buffer stream allows for both on-chip dilution and the separation of the enzyme and the substrate prior to droplet formation (to prevent the premature initiation of the reaction under study). As noted, droplets are formed using a flow-focusing geometry, where part of the continuous oil phase is diverted shortly before droplet formation (Figure S3A). Subsequently, the diverted oil is reintroduced into the primary flow, leading to an increase in the droplet velocity immediately after its formation. Downstream, a serpentine channel is used to ensure rapid mixing inside each droplet via chaotic advection. As droplets move along this channel, periodic stretching and reorientation of contained fluid lamina, combined with internal recirculation, results in an exponential decrease in the striation length over which mixing occurs (Figure S3).[22] Pressure-regulated drainage of oil through the side channels results in a rapid but controlled 8-fold decrease in the flow velocity. Additionally, with a view to increasing the observation time, the detection channel containing the decelerated droplets is extended by introduction of a series of switchbacks (Figure S4; Supplemental experimental procedure 3.11). Excitation light is focused into a line using an acylindrical lens, illuminating only 4.7 μm full width at half maximum (FWHM) stripe near the center of each droplet and greatly enhancing extractable fluorescence signals (Figures 2B and S5). Finally, dependent on the length of the detection channel, the maximum observation time could be varied to be between 300 and 1,000 ms.

To assess and quantify mixing efficiencies within droplets, we used the mass-transfer limited reaction between calcium ions with Fluo-4 (a fluorescence-based calcium-sensitive fluorophore).[22] Fluorescence images were acquired using 20 μs excitation pulses, with the signal being integrated over the entire droplet. This provides for a temporal resolution below 30 μs, when accounting for the droplet velocity and the

Please cite this article in press as: Hess et al., Exploring mechanism of enzyme catalysis by on-chip transient kinetics coupled with global data analysis and molecular modeling, Chem (2021), https://doi.org/10.1016/j.chempr.2021.02.011

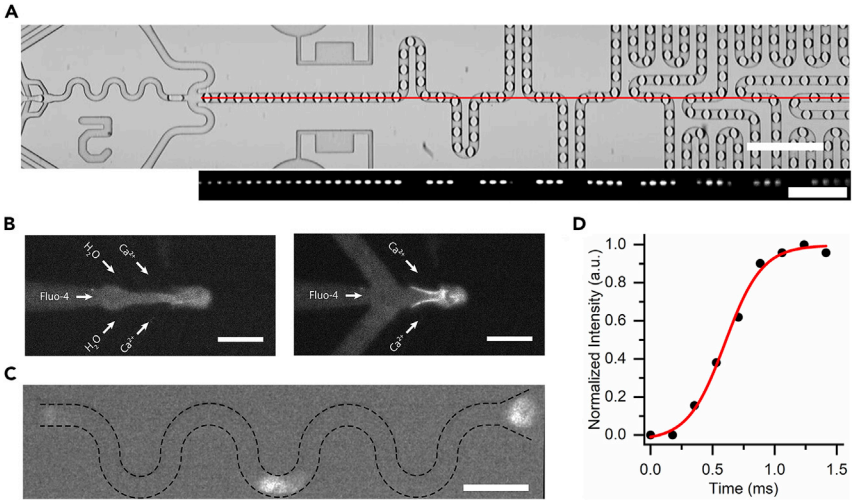

Figure 2. Operation of the high-throughput microfluidic platform for droplet formation and content mixing

(A) Top: bright-field image of the device in operation. The red line indicates the ROI used for detection. Scale bar: 400 μm. Bottom: fluorescence image showing microdroplets in the extended channel containing a fluorophore. Scale bar: 300 μm.

(B) Fluorescence images showing the formation of droplets containing Fluo-4 and calcium ions. The two reactants are separated by a calcium-free water stream (left), which prevents reaction prior to droplet formation. Conversely, the interfaces between the solutions light up in the absence of calcium-free water (right), indicating the start of the binding reaction.

(C) Fluorescence image of the mixing process. Scale bar: 100 μm.

(D) Representative measurement data, where 90% of the mixing takes place within 800 μs.

accuracy in determining the droplet position (± 5 μm). Figures 2B and 2C present fluorescence images of the droplet formation process and reaction between Fluo-4 (33 μM) and $CaCl_2$ (40 μM). While Fluo-4 is weakly fluorescent (Figure 2B), the Fluo-4/Ca^{2+} complex shows strong emission at 520 nm (Figure 2C). The variation of intensity as a function of time was modeled, as described previously.[13] Specifically, we define the time at which 50% of mixing is complete as the time at which an enzymatic reaction starts (t_0) and the time at which 90% mixing is complete as the time resolution of our system ($\Delta t_{mix,90\%}$). Mixing-time calculations for this reaction (Supplemental experimental procedure 3.10) assume $D_{Ca^{2+}} = 1.6 \times 10^{-9} m^2 s^{-1}$, droplet velocities between 0.8 and 1 ms^{-1}, and a channel width of 25 μm.[27] Based on this analysis, the time resolution of the microfluidic platform was found to be below 1 ms (Figure 2D).

Transient kinetics of model enzymes

We initially performed four different enzymatic assays to demonstrate the utility of the proposed microfluidic platform in measuring transient reaction kinetics. Importantly, the droplet-based microfluidic platform integrates a thin polydimethylsiloxane (PDMS) (500 μm) layer that covers the detection region and allows for precise focusing of the laser light sheet (Figures S2B and S5C; Supplemental experimental procedure 3.11). The single-turnover reaction kinetics of horseradish peroxidase (HRP) was initially studied by measuring the production of resorufin (increase of fluorescence) from the nonfluorescent reagents (Ampliflu Red [AR] and H_2O_2; Figure 3A). Using this fluorogenic reaction, we monitor the enzyme kinetics of HRP at single-turnover resolution, which typically exhibits a single-exponential time course. Second, investigation of the ferric microperoxidase (MP-11) mediated oxidation of AR by hydrogen peroxide (Figure S6A) evidenced a clear burst phase, reporting the

Please cite this article in press as: Hess et al., Exploring mechanism of enzyme catalysis by on-chip transient kinetics coupled with global data analysis and molecular modeling, Chem (2021), https://doi.org/10.1016/j.chempr.2021.02.011

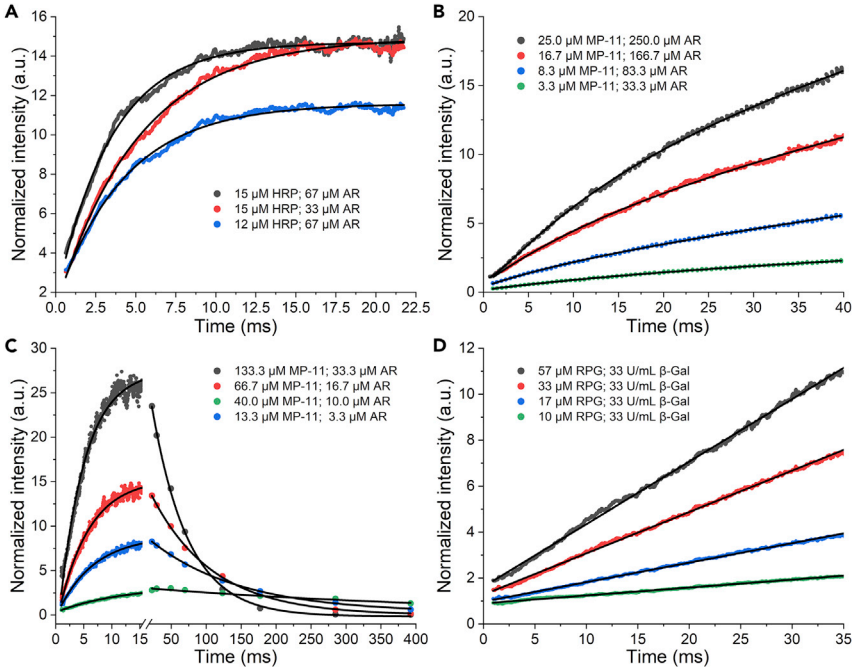

Figure 3. Kinetic data for four model enzymatic assays

(A) Increase in fluorescence resulting from the single-turnover reaction of HRP with the fluorogenic substrate AR was modeled using a single-exponential association function.

(B) MP-11 mediated oxidation reaction of a 10-fold excess of AR, initiated by the addition of 67 mM H_2O_2. After an initial burst phase, steady-state conditions were reached after approximately 20 ms. Linear fits are provided for the steady-state phase.

(C) MP-11 mediated oxidation of AR to resorufin (modeled with a single-exponential association function) and then to resazurin (highlighted by a single-exponential decrease in the fluorescence intensity) induced by the addition of 133 mM H_2O_2.

(D) For the reaction between 10 and 57 μM RGP with 33 U/mL β-galactosidase, an approximately linear increase in fluorescence is observed during the first 34 ms of the reaction. Each of the kinetic traces presented in (A), (B), and (D) was obtained by evaluating at least 1,000 images. The kinetic traces in (C) were obtained using ten droplets.

fast initial steps in the evolution of resorufin, followed by a slower step yielding a linear (steady-state) increase in fluorescence intensity (Figure 3B). Third, MP-11 mediated oxidation of AR (initially yielding resorufin, with further oxidation generating the nonfluorescent resazurin) was measured over an extended timescale (up to 400 ms). Significantly, we were able to measure the rapid evolution of resorufin, as well as isolating the significantly slower conversion step (Figure 3C). Finally, hydrolysis of resorufin β-D-galactopyranoside (RGP) by β-galactosidase (Figure S6B) indicated no visible pre-steady-state kinetic phase under the conditions used, with an approximately linear increase in the fluorescence intensity of resorufin as a function of time (Figures 3D and S7).

Transient kinetics and thermodynamics of haloalkane dehalogenase

We then used the microfluidic platform to conduct a kinetic and thermodynamic study of both natural and engineered variants of haloalkane dehalogenase, LinB, from *Shingobium japonicum* UT26. Haloalkane dehalogenases (HLDs) belong to the large group of structurally similar α/β-hydrolases that share a common fold (e.g., lipases, esterases, acetylcholinesterases, and carboxypeptidases) and are involved in numerous biotechnological applications.[28] More than three decades of experimental and *in silico* research on HLDs have made them benchmark enzymes

Please cite this article in press as: Hess et al., Exploring mechanism of enzyme catalysis by on-chip transient kinetics coupled with global data analysis and molecular modeling, Chem (2021), https://doi.org/10.1016/j.chempr.2021.02.011

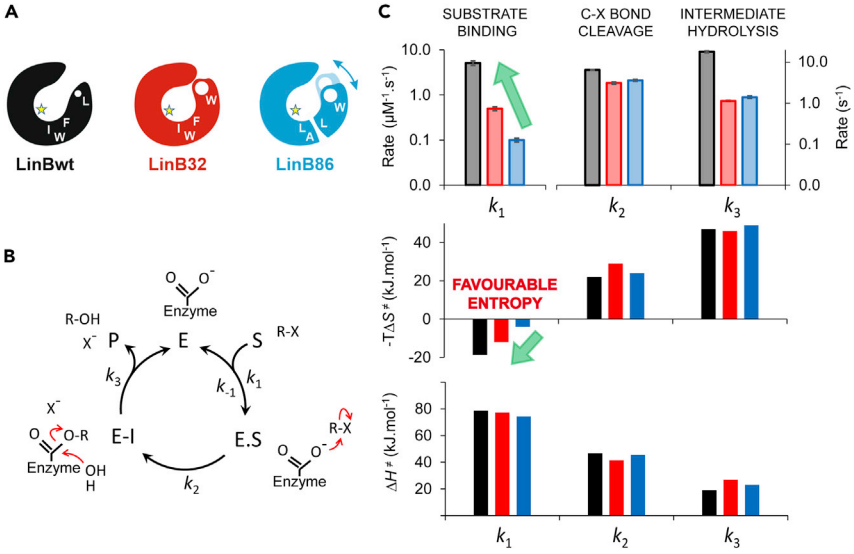

Figure 4. Kinetics and thermodynamics of LinB variants with engineered access tunnels

(A) Schematic illustration of access tunnels engineering, adopted from Kokkonen et al.[38] The main tunnel of LinBwt (black) playing a major role in the transport of ligands was significantly narrowed by introduction of a bulky Trp residue (W) into the bottleneck position 177 (red, LinB32). The subsequent mutations in the p3 region (F143L, W149A, and I211L) opened a new tunnel (blue, LinB86), resulting in the most proficient catalytic efficiency reported for haloalkane dehalogenase (k_{cat} = 57 s^{-1} observed with 1,2-dibromoethane at 37°C and pH 8.6).[28] The catalytic site is depicted by yellow star.

(B) The minimal model for the catalytic cycle of haloalkane dehalogenase LinB, adopted from Prokop et al.[37] The chemical mechanism is adopted from Verschueren et al.,[36] where R–X is halogenated substrate (X depicts Cl, Br, or I) and X– and R–OH are corresponding halide and alcohol products, respectively.

(C) The rate constants (upper panel) and thermodynamic parameters (middle and lower panel) for individual catalytic steps for the reaction of LinBwt (black), LinB32 (red) and LinB86 (blue) with Br-COU. The green arrows depict positive effect of entropy on the rate of substrate binding. Error bars represent standard error.

for studying structure-function relationships and the development of novel *in silico* methods in protein engineering.[29] Specifically, we examined LinBwt (PDB:1CV2) and two variants with engineered access tunnels, LinB32 (PDB:4WDQ) and LinB86 (PDB:4WDR) (Figure 4A). The entrance of the main tunnel was significantly narrowed by the introduction of a bulky tryptophan residue into the bottleneck position 177 (variant LinB32), resulting in a significant alteration of the kinetic characteristics for the conversion of small molecules, i.e., diminished catalytic efficiency, altered substrate specificity, and induced strong substrate inhibition.[30] Subsequent mutagenesis in the p3 region (F143L, W149A, and I211L) opened a new tunnel and introduced additional internal flexibility of the cap domain (variant LinB86), resulting in the most proficient haloalkane dehalogenase reported to date for the reaction with 1,2-dibromoethane (k_{cat} = 57 s^{-1} at 37°C and pH 8.6).[31] A fluorogenic substrate 4-(bromomethyl)-6,7-dimethoxycoumarin (Br-COU)[32] was employed as a "bulky" molecular probe to assess the effects of the tunnel engineering (Figures S8 and S9).

The ability to effectively perform complex kinetic and thermodynamic measurements required some modification to the core platform (Supplemental experimental procedures 3.12 and 3.13). First, upon prolonged operation, substrate molecules accumulate on and in the PDMS substrate, leading to increased background fluorescence signals. The partitioning of small, hydrophobic molecules into PDMS is a well-

Please cite this article in press as: Hess et al., Exploring mechanism of enzyme catalysis by on-chip transient kinetics coupled with global data analysis and molecular modeling, Chem (2021), https://doi.org/10.1016/j.chempr.2021.02.011

known phenomenon that can often be difficult to prevent.[33,34] Accordingly, the substrate material was changed from PDMS to a (tetrafluoroethylene- and hexafluoropropylene-based polymers) fluoroplastic via the adaptation of a protocol reported by Begolo et al. (Figures S10 and S11).[35] Additionally, the existence of slow phases for all reactions involving HLD variants made it necessary to extend the accessible observation time to several seconds, so that the measurement of complete catalytic cycles was possible. To this end, we designed a second microfluidic device to measure the slower kinetics of the LinB32 and LinB86 variants at the expense of slightly increased droplet wastage and slower mixing (Figure S11D; Supplemental experimental procedure 3.13). The design of the detection channel was identical for both types of devices, yielding a total length of 51.5 mm and nine interrogation points for measuring the reaction kinetics (Figure S12).

Single-turnover and multiple-turnover kinetic data were generated using both our microfluidic platform and a conventional stopped-flow instrument (Figures S13A, S13B, S15A, and S15B). On-chip experimentation allowed for a detailed study of temperature dependencies, due to reduced sample consumption, the ability to rapidly screen reaction conditions, and rapid temperature equilibration (obviating the need for preincubation of the unstable Br-COU molecule prior to measurement). Indeed, Br-COU is spontaneously hydrolyzed at elevated temperatures, making stopped-flow measurements at these conditions exceptionally difficult. Kinetic and thermodynamic parameters related to the individual steps of the catalytic cycle of LinB were subsequently analyzed by global analysis of the concentration- and temperature-dependent data using the kinetic pathway described previously (Figure 4B).[36,37]

The kinetic constants observed for the bulky Br-COU substrate (Figure 4C, upper panel; Table S1) are in contrast to results previously reported for the small substrates 1,2-dibromoethane, 1-bromohexane, and 1-chlorohexane.[37,38] The binding of bulky Br-COU, causing a greater range of van der Waals interactions with the enzyme, is a slow process, but one characterized by an affinity (K_S < 1 μM) two orders of magnitude higher than the rapid and significantly weaker binding observed for small substrates (K_S > 200 μM).[37,38] When compared with 1,2-dibromoethane, the tighter binding of Br-COU lowers the ground-state energy ($\Delta\Delta G^0$ 13 kJ.mol^{-1}) of the enzyme-substrate complex and thus contributes to the difference in the activation barrier ($\Delta\Delta G^{\neq}$ 7 kJ.mol^{-1}) for the following step, involving cleavage of the carbon-halogen bond (S_N2 reaction).[39] Interestingly, a positive entropic contribution offsets the enthalpy barrier associated with Br-COU binding (Figure 4C, middle and lower panels). The introduction of a Trp residue to LinB32 and LinB86 reduces the positive entropic ($\Delta\Delta S^{\neq}$) contribution to the binding of Br-COU by 7 and 15 kJ.mol^{-1}.K^{-1}, respectively, resulting in a decrease in the binding rate. Additionally, the rate limitation of the catalytic cycle changes as a result of engineering the access pathways. The rate of carbon-halogen bond cleavage (k_2) was indicated to limit conversion of Br-COU by LinBwt, while the rate of hydrolysis of the alkyl-enzyme intermediate (k_3) was slowest for both engineered variants, LinB32 and LinB86.

Molecular modeling

Molecular dynamics simulations were used to provide molecular insight into the specificity of variants with engineered entrance tunnels. Multiple binding events of Br-COU were observed during the 500*50 ns (25 μs) simulations, allowing the construction of Markov state models for the binding event (Supplemental experimental procedure 3.9). Five Markov states constructed from the contact map of the heavy atoms of Br-COU and Cα atoms revealed that Br-COU binds differently with the

Please cite this article in press as: Hess et al., Exploring mechanism of enzyme catalysis by on-chip transient kinetics coupled with global data analysis and molecular modeling, Chem (2021), https://doi.org/10.1016/j.chempr.2021.02.011

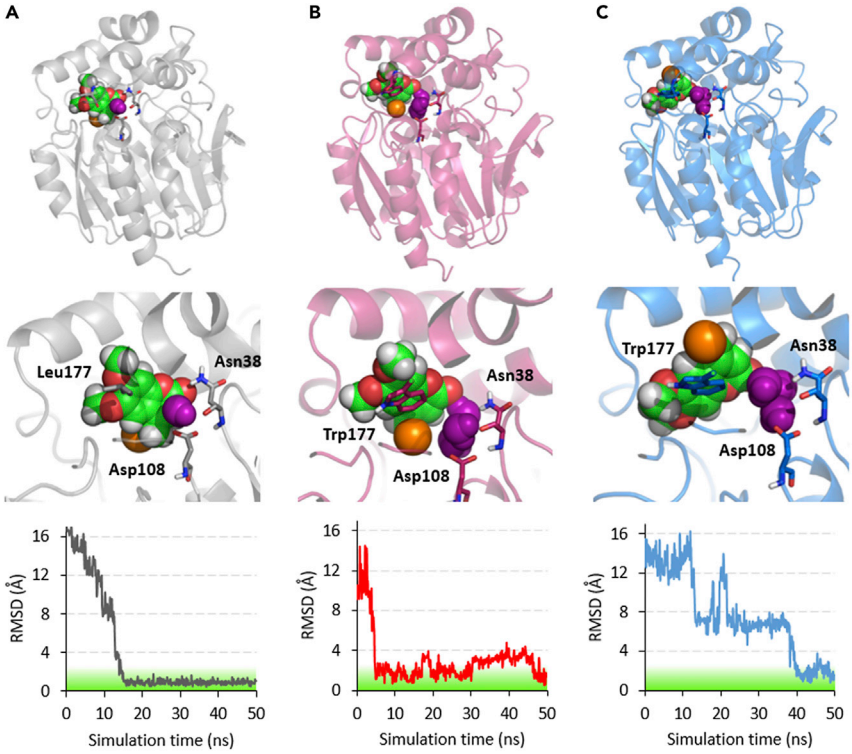

Figure 5. Structural models of enzyme-substrate complexes obtained by molecular dynamics simulations

(A–C) Representative binding modes observed during the molecular dynamics simulations for (A) LinBwt, (B) LinB32, and (C) LinB86. Top images show the overview of the enzyme with the bound substrate. Middle images show close ups of the bound substrate (spheres, where green represents carbon; red, oxygen; white, hydrogen; bromine, orange) with the catalytic residues (sticks) and bound water molecules (purple). The bottom plots shows the RMSD values for the heavy atoms of the ligand related to the most common bound state (depicted on the top part of the figure), as calculated from a single 50-ns simulation. A stable RMSD of <2 Å indicates that the substrate is tightly bound and is not moving from its position, and to highlight this the 0–2 Å area of the graph has a green background.

individual variants. Whereas the bound clusters for LinB32 and LinB86 do not display a single (preferred) binding orientation inside the active site, a well-defined cluster is observed for LinBwt (Table S2), with Br-COU adopting a tightly bound binding pose (Figure 5A). On the contrary, such a stable binding pose is not observed in LinB32 and LinB86, with Br-COU tending to change orientation continuously. In the tightly bound pose of LinBwt, Br-COU has displaced all but one water molecule from the pocket, while two or three water molecules are present in similar bound poses in LinB32 and LinB86 (Figures 5A–5C). Unlike smaller substrates, Br-COU appears to bind to the active site with its carbonyl oxygen between the halide-stabilizing residues, a conformation which has not been previously observed. The lack of the traditional binding mode and the high affinity of LinBwt for Br-COU both suggest that the binding mode with carbonyl oxygen in between the halide-stabilizing residues is a productive one, but one that results in a higher barrier for the S_N2 reaction.

Even though Br-COU is much larger than the natural substrates of LinB, the molecule stays in a planar configuration due to its aromatic structure, with the protein not undergoing large conformational changes upon binding. In LinBwt, Br-COU displaces two of the three residual water molecules (Figure 5A). It is beneficial for the binding

Please cite this article in press as: Hess et al., Exploring mechanism of enzyme catalysis by on-chip transient kinetics coupled with global data analysis and molecular modeling, Chem (2021), https://doi.org/10.1016/j.chempr.2021.02.011

entropy to release tightly bound water molecules from the protein cavity, since they will have more hydrogen-bonding orientations in the bulk solvent.[40] The displacement of a water molecule contributes between −2 and −11 kJ.mol^{-1} to the binding entropy.[41,42] Accordingly, the observed displacement of two additional water molecules could contribute between −4 and −22 kJ.mol^{-1} to the entropy of COU-Br binding to LinBwt, a value that is in good agreement with the experimental findings herein (Figure 4C). In LinB32 and LinB86, the bulky Trp177 hinders the release of water molecules through the tunnel and prevents a tight binding of Br-COU (Figures 5B and 5C). Moreover, root-mean-square-deviation (RMSD) graphs demonstrate that kinetic differences in binding can be explained by the stability of the bound form (Figure 5). In LinBwt, the most common binding mode is stable, whereas in LinB32 and LinB86, both the water molecules and the Trp177 cause bound Br-COU to explore different conformations.

DISCUSSION

Herein, we have reported the development, characterization, and application of a droplet-based microfluidic platform for the analysis of information-rich transient phases of enzymatic reactions. Experiments performed within the current study include temperature-dependent single- and multiple-turnover measurements, which have been used to extract kinetic and thermodynamic parameters for individual catalytic steps of a complex reaction. In this regard, it is particularly advantageous that the microfluidic platform does not require any preheating of enzymatic samples solutions prior to experiment, since heating takes place within the device and on very short timescales. This in turn enables measurements near enzyme melting temperatures, without inducing substantial denaturation.

Specifically, we have demonstrated the use of the microfluidic platform to gather large sets of temperature- and concentration-dependent (transient) kinetic data. The collected datasets were used to calculate detailed kinetic and thermodynamic parameters via global data analysis, where multiple data sets were simultaneously fit to a single model using numerical integration. Experimental results in conjunction with molecular dynamics simulations provided detailed new information regarding the mechanisms governing the catalytic efficiency and substrate specificity of both native and engineered enzyme variants. Significantly, results indicate that the same enzyme structure can enforce distinct mechanisms to secure efficient specificity toward structurally different substrates. While the specificity toward bulky Br-COU is driven by the formation of the strong enzyme-substrate complex, enzyme saturation with the small, weakly bound 1,2-dibromoethane is driven by a fast chemical step.[37] Such an analysis revealed that a positive gain in entropy is a critical factor for Br-COU binding and connected with desolvation of the active site cavity by this bulky substrate. In the engineered variants, the introduced Trp177 residue hinders the exit of water molecules and provides an experimental estimate for entropic contributions to Br-COU binding (up to 15 kJ.mol^{-1}) related to active site desolvation. The rate of the following chemical step, S_N2 cleavage of the carbon-halogen bond, is slow for the reaction of Br-COU. This can be attributed to the lower ground-state energy of the tight enzyme-substrate complex and to the unusual orientation of the halide-leaving group. The kinetic and thermodynamic data amassed using the current microfluidic platform provided essential input for molecular dynamics simulations. Under normal circumstances, the definition of starting parameters (such as temperature, ionic strength, and ligand concentrations) is not a straightforward process. Despite the fact that molecular dynamics simulations can be enormously useful in providing molecular details of the recognition of small molecules by interacting

Please cite this article in press as: Hess et al., Exploring mechanism of enzyme catalysis by on-chip transient kinetics coupled with global data analysis and molecular modeling, Chem (2021), https://doi.org/10.1016/j.chempr.2021.02.011

proteins, conformational changes, or the role of solvent, biologically interpretable results can be obtained only when the initial system conditions are properly set using experimental data. In this way, molecular dynamics simulations act as a complementary information tool to interpret experimental observations, in the current study rationalizing experimental observations from a structural perspective. Furthermore, experimental (kinetic and thermodynamic) data may also benchmark and validate results provided by molecular dynamics simulations.

The current study has also demonstrated that the engineering of access pathways can induce a shift in the rate limitation. For example, the carbon-halogen bond cleavage was indicated as rate limiting for LinBwt, whereas hydrolysis became rate limiting for LinB32 and LinB86, a variation that is most likely linked to restricted transport of the water molecules. A similar phenomenon has been previously observed for engineering access tunnels of haloalkane dehalogenase DhaA from *Rhodococcus rhodochrous*, leading to active site (de)solvation associated with the enhanced velocity of the chemical steps and accompanied by a switch in the rate limitation.[43] In summary, this study confirms the importance of access pathways for transport of ligands, but interestingly shows that their modification can significantly also affect chemical steps, connected with active site (de)solvation; a far less intuitive observation.[44–46]

The global kinetic and thermodynamic analysis presented herein has made it possible to decipher the nature of catalytic efficiency and substrate specificity of the studied hydrolytic enzymes that represent over 100,000 members of α/β-hydrolase superfamily. Traditionally, quantitative thermodynamic determinants are extremely difficult to obtain using conventional techniques. Here, knowledge of the mechanism and thermodynamic terms for enzyme-substrate recognition are critical when selecting the proper strategy for rational engineering of targeted enzyme specificity. In this regard, our droplet-based microfluidic method, for high-throughput screening of transient kinetics at different reactant concentrations and temperatures, can be used to investigate the thermodynamic properties of many other enzymatic reaction systems.

Importantly, the system is capable of tracking single droplets and, thus, has obvious utility in the measurement of rapid reactions in a wide range of other applications, where traditional stopped-flow measurements are compromised or difficult to perform. For example, our approach is well-suited to the investigation of membrane-based enzymes, which are vulnerable to the high shear forces, developed in turbulent mixers and stopped-flow instruments.[47] An obvious additional application of the described platform is in the study of rapid polymerization reactions.[48,49] Here, droplets provide an ideal reaction environment, since they prevent contact between the polymerizing solution and channel walls. Moreover, since different positions along the flow path correspond to different times after reaction initiation, extended integration times may be accessed without any compromise to temporal resolution.[22] This opens up the possibility of monitoring transient events using information-rich, time-resolved spectroscopies (such as time-resolved fluorescence and time-resolved fluorescence anisotropy), which is not feasible within conventional stopped-flow instruments.

A primary drawback associated with conventional stopped-flow instrumentation relates to the need for unacceptably large sample/reagent volumes. This is especially problematic when performing single-turnover experiments where enzyme should be present in excess over substrate. Droplet-based microfluidic systems provide a

Please cite this article in press as: Hess et al., Exploring mechanism of enzyme catalysis by on-chip transient kinetics coupled with global data analysis and molecular modeling, Chem (2021), https://doi.org/10.1016/j.chempr.2021.02.011

significant advantage when performing enzymatic reactions, since they operate at high throughput, consume miniscule volumes of sample/reagent, and are able to probe reaction parameter space in a rapid and efficient manner. Our microfluidic platform is adept at generating large sequences of droplets with user-defined payloads. Moreover, the use of stroboscopic epifluorescence imaging allows the efficient interrogation and tracking of individual droplets with high spatial and temporal resolution and the subsequent extraction of kinetic information at the single droplet level. It should also be remembered that a primary feature of microfluidic segmented flows is rapid heat transfer, which engenders almost instantaneous temperature equilibration of the fluid flow and the precise control of temperature over different experiments. Put simply, we believe that the presented platform represents a powerful new tool for efficient and systematic collection of comprehensive kinetic data, enabling a better understanding of enzyme evolution and providing new strategies for rational protein engineering.

EXPERIMENTAL PROCEDURES

Resource availability

Lead contact

Further information and requests for resources should be directed to and will be fulfilled by the Lead Contact, Andrew deMello (andrew.demello@chem.ethz.ch).

Materials availability

This study did not generate new unique reagents.

Data and code availability

The datasets supporting the current study have not been deposited in a public repository but are available from the corresponding author on request.

Microfluidic device fabrication

Microfluidic channel patterns were designed using AutoCAD (AutoCAD 2017, Autodesk, San Rafael CA, USA) and printed onto transparent film masks (Micro Lithography Services, Chelmsford, United Kingdom). Master SU-8 molds on silicon wafers (with feature heights of 33 $\pm$ 2 μm) were created using conventional photolithographic techniques. Microfluidic devices were fabricated using standard soft-lithographic techniques described in detail in the Supplemental experimental procedures 3.1 and 3.2.

Microfluidic device operation

Precision neMESYS syringe pumps (CETONI GmbH, Korbussen, Germany) were used to provide for precise control of fluid flow rates. For devices operating under controlled back-pressure conditions (i.e., to regulate oil drainage), the appropriate outlet was connected to a Mitos pressure pump (Dolomite Centre, Royston, United Kingdom) applying a positive pressure of 250 mbar. HFE-7500 (3M, Minnesota, USA) oil containing 1% (w/w) of fluorosurfactant (RAN Biotechnologies, Massachusetts, United States) was used as the continuous phase in all experiments. For experiments with model enzymes, the flow rate of the continuous phase was typically set to 33 μL/min and the total flow rate of the aqueous flows was 3 μL/min. For experiments with the wild type enzyme, oil phase flow rates were set between 22 and 24 μL/min, and for experiments with enzyme variants, oil phase flow rates between 1.5 and 3.5 μL/min were used. The total aqueous flow rate in all experiments was 1 μL/min.

Please cite this article in press as: Hess et al., Exploring mechanism of enzyme catalysis by on-chip transient kinetics coupled with global data analysis and molecular modeling, Chem (2021), https://doi.org/10.1016/j.chempr.2021.02.011

Reaction temperatures were controlled by attaching microfluidic devices to a bespoke heating stage (Figure S2B). A 1 mm wide slit in the middle of heating stage allowed facile observation of droplets when using a microscope objective (Plan Apo 4x/ NA 0.2, Nikon, Zurich, Switzerland). To quantify on-chip temperatures and assess thermal homogeneity within the detection area, 500 μm holes were drilled at five different positions around the detection channel and 5211 module thermocouples (National Instrument, Austin, USA) inserted under varying conditions. The obtained calibration curve is shown in Figure S8B. For temperature-dependent kinetic experiments, measurements at the lowest temperature were made first and followed by stepwise increments of between 2°C and 4°C, with an equilibration period of 3 min between measurements.

On-chip assays

All assays were conducted at 20°C unless otherwise stated and all solutions were passed through a 0.45 μm PTFE filter (Fisher Scientific, Reinach, Switzerland) prior to use. The mixing assay was performed in 20 mM phosphate-buffered saline at pH 7.2 (Sigma-Aldrich, Buchs, Switzerland) containing 2 μM EDTA (Sigma-Aldrich, Buchs, Switzerland) to chelate residual calcium ions. Individual syringes were loaded with buffer solution, a 100 μM Fluo-4 (Thermo Fisher Scientific, Basel, Switzerland) solution, and a 120 μM $CaCl_2$ solution (Sigma-Aldrich, Buchs, Switzerland). Further details regarding reagents, sample preparation, and enzymatic assay conditions are provided in Supplemental experimental procedures 3.3 and 3.4.

Optical setup and data acquisition

The optical system comprised a Nikon Ti-E inverted microscope (Nikon, Zurich, Switzerland) equipped with a motorized positioning stage (Mad City Labs, Madison, USA). 488 nm (Sapphire 488 LP, Coherent, Ely, United Kingdom), 532 nm (Sapphire 532 LP, Coherent, Ely, United Kingdom), and 375 nm (PhoxX plus 375-70, Omicron-Laserage, Rodgau-Dudenhofen, Germany) excitation laser beams were combined using a set of dichroic mirrors. Further details regarding the optical set up are provided in the Supplemental experimental procedure 3.5.

Image processing and data analysis

ImageJ (National Institutes of Health, USA) was used for all image processing tasks. Details of all image analysis procedures are provided in the Supplemental experimental procedure 3.6 and Figure S17.

Stopped-flow measurements

Conventional rapid-mixing experiments were conducted using a SFM 300 stopped-flow instrument equipped with a MOS-500 spectro-polarimeter (Biologic, Seyssinet-Pariset, France). A 435 nm long-pass filter was employed to isolate and collect emitted light. Single and multiple-turnover conditions were used to obtain information regarding all kinetically significant steps as well as to examine any dependency on substrate concentration. Further details are provided in the Supplemental experimental procedure 3.7.

Kinetic data analysis and statistics

Single and multiple-turnover kinetic data obtained via stopped-flow measurements (at 30°C) and the microfluidic system collected (at temperatures between 298.6 and 326.2 K) were fitted globally using the *KinTek Global Kinetic Explorer* dynamic kinetic simulation software (KinTek Corporation, PA, USA), to extract temperature-dependent rate constants.[50] Further details of data fitting procedures are provided in the Supplemental experimental procedure 3.8.

Molecular dynamics simulations

The system was equilibrated at 300K for 5 ns using the Equilibration_v2 protocol of high-throughput molecular dynamics (HTMD) and the default parameters associated with the AceMD software.[51] Production simulations were run as adaptive epochs at 300 K and using the default parameters of the Production_v6 protocol of HTMD. The metric used in the adaptive sampling was the distance between the heavy atoms of Br-COU and Trp residues and the Cα of the halide-stabilizing Trp109 and Asp147 (at the tunnel mouth). The total simulation time was 500*50 ns (25 μs) for all variants. Simulations were analyzed using Markov state models. Further details are provided in Supplemental experimental procedure 3.9, Figure S16, and Tables S2 and S3.

SUPPLEMENTAL INFORMATION

Supplemental information can be found online at https://doi.org/10.1016/j.chempr.2021.02.011.

ACKNOWLEDGMENTS

The authors would like to acknowledge support from the Swiss National Science Foundation (grant number: 205321/176011/1), ETH Research Grant (grant number: ETH-02 14-1), the CETOCOEN EXCELLENCE Teaming 2 project supported by the Horizon 2020 Program (857560), and the Czech Ministry of Education, Youth and Sports (02.1.01/0.0/0.0/18_046/0015975). The work was also supported by the Operational Program Research, Development and Education Project, MSCA fellow @ MUNI" (CZ.02.2.69/0.0/0.0/17_050/0008496) and the RECETOX research infrastructure of the Czech Ministry of Education, Youth and Sports (LM2018121).

AUTHOR CONTRIBUTIONS

A.d.M., S.S., D.H., and Z.P. conceived the project and devised the research plan. D.H. developed the instrumental platform and methodology, while D.H. and V.D. performed all experiments. D.H. performed image processing, Z.P. and J.D. performed data analysis, P.K. and D.B. performed molecular dynamic simulations with V.D, and J.D. and Z.P. developed the enzyme purification protocols. D.H, A.d.M., S.S., and Z.P. wrote the manuscript.

DECLARATION OF INTERESTS

The authors declare no competing interests.

Received: October 21, 2020
Revised: December 18, 2020
Accepted: February 10, 2021
Published: March 9, 2021

REFERENCES

1. Wohlgemuth, R. (2010). Biocatalysis—key to sustainable industrial chemistry. Curr. Opin. Biotechnol. *21*, 713–724.
2. Agrawal, N.V., and Patil, N.A. (2020). Enzyme technology prospects and their biomedical applications. In Advances in Bioengineering, R. Vyas, ed. (Springer), pp. 147–159.
3. Hauer, B. (2020). Embracing nature's catalysts: a viewpoint on the future of biocatalysis. ACS Catal. *10*, 8418–8427.
4. Wu, S., Snajdrova, R., Moore, J.C., Baldenius, K., and Bornscheuer, U.T. (2021). Biocatalysis: enzymatic synthesis for industrial applications. Angew. Chem. Int. Ed. Engl. *60*, 88–119.
5. Chen, K., and Arnold, F.H. (2020). Engineering new catalytic activities in enzymes. Nat. Cat. *3*, 203–213.
6. Bornscheuer, U.T., Huisman, G.W., Kazlauskas, R.J., Lutz, S., Moore, J.C., and Robins, K. (2012). Engineering the third wave of biocatalysis. Nature *485*, 185–194.
7. Bornscheuer, U.T. (2018). The fourth wave of biocatalysis is approaching. Philos. Trans. A Math. Phys. Eng. Sci. *376*, 20170063.
8. Sheldon, R.A., and Pereira, P.C. (2017). Biocatalysis engineering: the big picture. Chem. Soc. Rev. *46*, 2678–2691.
9. Johnson, K.A. (1998). Advances in transient-state kinetics. Curr. Opin. Biotechnol. *9*, 87–89.
10. Li, A., Ziehr, J.L., and Johnson, K.A. (2017). A new general method for simultaneous fitting of

temperature and concentration dependence of reaction rates yields kinetic and thermodynamic parameters for HIV reverse transcriptase specificity. J. Biol. Chem. *292*, 6695–6702.

11. Hartwell, S.K., and Grudpan, K. (2012). Flow-based systems for rapid and high-precision enzyme kinetics studies. J. Anal. Methods Chem. *2012*, 450716.

12. Han, Z., Li, W., Huang, Y., and Zheng, B. (2009). Measuring rapid enzymatic kinetics by electrochemical method in droplet-based microfluidic devices with pneumatic valves. Anal. Chem. *81*, 5840–5845.

13. Song, H., and Ismagilov, R.F. (2003). Millisecond kinetics on a microfluidic chip using nanoliters of reagents. J. Am. Chem. Soc. *125*, 14613–14619.

14. deMello, A.J. (2006). Control and detection of chemical reactions in microfluidic systems. Nature *442*, 394–402.

15. Rho, H.S., Hanke, A.T., Ottens, M., and Gardeniers, H. (2016). Mapping of enzyme kinetics on a microfluidic device. PLoS One *11*, e0153437.

16. Sjostrom, S.L., Joensson, H.N., and Svahn, H.A. (2013). Multiplex analysis of enzyme kinetics and inhibition by droplet microfluidics using picoinjectors. Lab Chip *13*, 1754–1761.

17. Ristenpart, W.D., Wan, J., and Stone, H.A. (2008). Enzymatic reactions in microfluidic devices: Michaelis–Menten kinetics. Anal. Chem. *80*, 3270–3276.

18. Simon, M.G., and Lee, A.P. (2012). Microfluidic droplet manipulations and their applications. In Microdroplet Technology: Principles and Emerging Applications in Biology and Chemistry, P. Day, A. Manz, and Y. Zhang, eds. (Springer), pp. 23–50.

19. Song, H., Chen, D.L., and Ismagilov, R.F. (2006). Reactions in droplets in microfluidic channels. Angew. Chem. Int. Ed. Engl. *45*, 7336–7356.

20. Borgia, M.B., Borgia, A., Best, R.B., Steward, A., Nettels, D., Wunderlich, B., Schuler, B., and Clarke, J. (2011). Single-molecule fluorescence reveals sequence-specific misfolding in multidomain proteins. Nature *474*, 662–665.

21. Krishnadasan, S., Brown, R.J.C., deMello, A.J., and deMello, J.C. (2007). Intelligent routes to the controlled synthesis of nanoparticles. Lab Chip *7*, 1434–1441.

22. Song, H., Tice, J.D., and Ismagilov, R.F. (2003). A microfluidic system for controlling reaction networks in time. Angew. Chem. Int. Ed. Engl. *42*, 768–772.

23. Huebner, A.M., Abell, C., Huck, W.T.S., Baroud, C.N., and Hollfelder, F. (2011). Monitoring a reaction at submillisecond resolution in picoliter volumes. Anal. Chem. *83*, 1462–1468.

24. Bleul, R., Ritzi-Lehnert, M., Höth, J., Scharpfenecker, N., Frese, I., Düchs, D., Brunklaus, S., Hansen-Hagge, T.E., Meyer-Almes, F.J., and Drese, K.S. (2011). Compact, cost-efficient microfluidics-based stopped-flow device. Anal. Bioanal. Chem. *399*, 1117–1125.

25. Li, Y., Zhang, D., Feng, X., Xu, Y., and Liu, B.F. (2012). A microsecond microfluidic mixer for characterizing fast biochemical reactions. Talanta *88*, 175–180.

26. Song, H., Bringer, M.R., Tice, J.D., Gerdts, C.J., and Ismagilov, R.F. (2003). Experimental test of scaling of mixing by chaotic advection in droplets moving through microfluidic channels. Appl. Phys. Lett. *83*, 4664–4666.

27. Bringer, M.R., Gerdts, C.J., Song, H., Tice, J.D., and Ismagilov, R.F. (2004). Microfluidic systems for chemical kinetics that rely on chaotic mixing in droplets. Philos. Trans. A Math. Phys. Eng. Sci. *362*, 1087–1104.

28. Koudelakova, T., Bidmanova, S., Dvorak, P., Pavelka, A., Chaloupkova, R., Prokop, Z., and Damborsky, J. (2013). Haloalkane dehalogenases: biotechnological applications. Biotechnol. J. *8*, 32–45.

29. Damborsky, J., Chaloupkova, R., Pavlova, M., Chovancova, E., and Brezovsky, J. (2010). Structure-function relationships and engineering of haloalkane dehalogenases. In Handbook of Hydrocarbon and Lipid Microbiology, K.N. Timmis, ed. (Springer), pp. 1081–1098.

30. Biedermannová, L., Prokop, Z., Gora, A., Chovancová, E., Kovács, M., Damborský, J., and Wade, R.C. (2012). A single mutation in a tunnel to the active site changes the mechanism and kinetics of product release in haloalkane dehalogenase LinB. J. Biol. Chem. *287*, 29062–29074.

31. Brezovsky, J., Babkova, P., Degtjarik, O., Fortova, A., Gora, A., Iermak, I., Rezacova, P., Dvorak, P., Smatanova, I.K., Prokop, Z., et al. (2016). Engineering a de novo transport tunnel. ACS Catal. *6*, 7597–7610.

32. Dockalova, V., Sanchez-Carnerero, E.M., Dunajova, Z., Palao, E., Slanska, M., Buryska, T., Damborsky, J., Klán, P., and Prokop, Z. (2020). Fluorescent substrates for haloalkane dehalogenases: novel probes for mechanistic studies and protein labeling. Comput. Struct. Biotechnol. J. *18*, 922–932.

33. Toepke, M.W., and Beebe, D.J. (2006). PDMS absorption of small molecules and consequences in microfluidic applications. Lab Chip *6*, 1484–1486.

34. Domansky, K., Leslie, D.C., McKinney, J., Fraser, J.P., Sliz, J.D., Hamkins-Indik, T., Hamilton, G.A., Bahinski, A., and Ingber, D.E. (2013). Clear castable polyurethane elastomer for fabrication of microfluidic devices. Lab Chip *13*, 3956–3964.

35. Begolo, S., Colas, G., Viovy, J.L., and Malaquin, L. (2011). New family of fluorinated polymer chips for droplet and organic solvent microfluidics. Lab Chip *11*, 508–512.

36. Verschueren, K.H.G., Seljée, F., Rozeboom, H.J., Kalk, K.H., and Dijkstra, B.W. (1993). Crystallographic analysis of the catalytic mechanism of haloalkane dehalogenase. Nature *363*, 693–698.

37. Prokop, Z., Monincová, M., Chaloupková, R., Klvana, M., Nagata, Y., Janssen, D.B., and Damborský, J. (2003). Catalytic mechanism of the maloalkane dehalogenase LinB from Sphingomonas paucimobilis UT26. J. Biol. Chem. *278*, 45094–45100.

38. Kokkonen, P., Sykora, J., Prokop, Z., Ghose, A., Bednar, D., Amaro, M., Beerens, K., Bidmanova, S., Slanska, M., Brezovsky, J., et al. (2018). Molecular gating of an engineered enzyme captured in real time. J. Am. Chem. Soc. *140*, 17999–18008.

39. Fersht, A. (2017). Structure and Mechanism in Protein Science (World Scientific).

40. Gerogiokas, G., Southey, M.W.Y., Mazanetz, M.P., Heifetz, A., Bodkin, M., Law, R.J., and Michel, J. (2015). Evaluation of water displacement energetics in protein binding sites with grid cell theory. Phys. Chem. Chem. Phys. *17*, 8416–8426.

41. Huggins, D.J. (2015). Quantifying the entropy of binding for water molecules in protein cavities by computing correlations. Biophys. J. *108*, 928–936.

42. Yu, H.T., and Rick, S.W. (2010). Free energy, entropy, and enthalpy of a water molecule in various protein environments. J. Phys. Chem. B *114*, 11552–11560.

43. Pavlova, M., Klvana, M., Prokop, Z., Chaloupkova, R., Banas, P., Otyepka, M., Wade, R.C., Tsuda, M., Nagata, Y., and Damborsky, J. (2009). Redesigning dehalogenase access tunnels as a strategy for degrading an anthropogenic substrate. Nat. Chem. Biol. *5*, 727–733.

44. Kokkonen, P., Bednar, D., Pinto, G., Prokop, Z., and Damborsky, J. (2019). Engineering enzyme access tunnels. Biotechnol. Adv. *37*, 107386.

45. Hendil-Forssell, P., Martinelle, M., and Syrén, P.O. (2015). Exploring water as building bricks in enzyme engineering. Chem. Commun. (Camb). *51*, 17221–17224.

46. Magdziarz, T., Mitusińska, K., Gołdowska, S., Płuciennik, A., Stolarczyk, M., Ługowska, M., and Góra, A. (2017). Aqua-DUCT: a ligands tracking tool. Bioinformatics *33*, 2045–2046.

47. Thomas, C.R., and Geer, D. (2011). Effects of shear on proteins in solution. Biotechnol. Lett. *33*, 443–456.

48. Ozyamak, E., Kollman, J., Agard, D.A., and Komeili, A. (2013). The bacterial actin MamK: in vitro assembly behavior and filament architecture. J. Biol. Chem. *288*, 4265–4277.

49. Thakur, A., Wada, T., Chammingkwan, P., Terano, M., and Taniike, T. (2019). Development of large-scale stopped-flow technique and its application in elucidation of initial Ziegler–Natta olefin polymerization kinetics. Polymers *11*, 1012.

50. Johnson, K.A., Simpson, Z.B., and Blom, T. (2009). Global Kinetic Explorer: A new computer program for dynamic simulation and fitting of kinetic data. Anal. Biochem. *387*, 20–29.

51. Harvey, M.J., Giupponi, G., and Fabritiis, G.D. (2009). ACEMD: accelerating BioMolecular dynamics in the microsecond time scale. J. Chem. Theor. Comput. *5*, 1632–1639.